

Article

Laser In Situ U–Pb Isotope Dating of Carbonate Rocks in Weijia Guyot in the Western Pacific Ocean and Its Geological Significance

Zhenquan Wei ^{1,2}, Jinfeng Ma ^{1,2,*}, Gaowen He ^{1,2}, Lifeng Zhong ³, Limin Zhang ^{1,2}  and Bin Zhao ^{1,2} 

¹ Key Laboratory of Marine Resources, Ministry of Natural Resources, Guangzhou Marine Geological Survey, China Geological Survey, Guangzhou 510075, China; wei_zhenquan@163.com (Z.W.); hgaowen@mail.cgs.gov.cn (G.H.); zhanglm8@mail2.sysu.edu.cn (L.Z.); zbin_a@mail.cgs.gov.cn (B.Z.)

² Southern Marine Science and Engineering Guangdong Laboratory (Guangzhou), Guangzhou 511458, China

³ Southern Marine Science and Engineering Guangdong Laboratory (Zhuhai), Zhuhai 519080, China; zhonglifeng@sml-zhuhai.cn

* Correspondence: guai99@163.com

Abstract: Shallow-water carbonate rocks constitute a crucial component of large guyots, arising in distinct environments and harboring valuable insights into the evolutionary stages of seamount islands as well as the tectonic conditions of the underlying oceanic plate. Laser Ablation Multi-Collector Inductively Coupled Plasma Mass Spectrometry (LA-MC-ICP-MS) was used to conduct in situ U–Pb isotope dating of carbonate minerals with low uranium content collected from Weijia Guyot. This dating approach yielded crucial evidence for the vertical development of the seamount. Our study indicates that shallow-water carbonate rocks in Weijia Guyot had a temporal range between 91 My and 137 My. The carbonate rocks underwent two growth phases, Hauterivian to Barremian and Cenomanian to Turonian, with a hiatus of approximately 20 My. Since the Hauterivian age, the shield volcano of Weijia Guyot is essentially complete, with its seamount top exposed at or near sea level and receiving its first stage of shallow-water carbonate sedimentation. Based on the dating of both shallow-water carbonate rocks and hawaiiite within the Weijia Guyot, it is inferred that approximately 10 My elapsed from shield-building volcanism to late alkalic volcanism. During the Turonian age, the main reason for the second phase of shallow-water carbonate rocks in the seamounts was the regional tectonic uplift triggered by the drift of the Weijia Guyot along with the Pacific Plate toward the Society hotspot.

Keywords: carbonate rocks; in situ U–Pb isotope dating; tectonic evolution; Weijia Guyot; Western Pacific Ocean



Citation: Wei, Z.; Ma, J.; He, G.; Zhong, L.; Zhang, L.; Zhao, B. Laser In Situ U–Pb Isotope Dating of Carbonate Rocks in Weijia Guyot in the Western Pacific Ocean and Its Geological Significance. *J. Mar. Sci. Eng.* **2024**, *12*, 737. <https://doi.org/10.3390/jmse12050737>

Academic Editor: Gary Wilson

Received: 25 March 2024

Revised: 26 April 2024

Accepted: 26 April 2024

Published: 28 April 2024



Copyright: © 2024 by the authors. Licensee MDPI, Basel, Switzerland. This article is an open access article distributed under the terms and conditions of the Creative Commons Attribution (CC BY) license (<https://creativecommons.org/licenses/by/4.0/>).

1. Introduction

Seamounts are widely distributed in various ocean basins worldwide [1–9]. Some have abundant Co-rich crust and fishery resources and are repositories for marine life and microorganisms [10–18]. In addition, seamounts are key points of intersection between the biosphere, hydrosphere, and lithosphere, and are globally relevant [19].

Seamount formation and evolution begin due to submarine volcanism [19,20] and expand as magmatic activity continues. When an evolving seamount reaches a water depth of 700 m or less, eruption intensity increases sharply due to the relatively low seawater pressure. Eventual emergence above sea level provides substrates for carbonate reefs, ranging from minor shoreline reefs to massive coral reefs, that may cover the entire subsiding volcano. Once the volcanism ceases, the volcanic island will eventually drown due to erosion and subsidence [19]. When coral reefs grow slower than the subsidence of volcanic islands, coral reefs sink below the photic zone and eventually die. Former islands and coral reefs have become seamounts with flat tops (namely guyots) through

these geological processes [20]. When a seamount reaches a subduction zone, or when the ocean basin it is located in closes due to the collision of two continental plates on both sides of the ocean, its life cycle ends.

In addition to volcanic bases, carbonate reefs, and their related sedimentary rocks are also important seamount components. These rocks originated from distinct environments and serve as repositories for crucial data pertaining to seamount evolutionary stages and the tectonic conditions of the underlying ocean plate. The isotopic chronology of carbonate minerals helps elucidate the evolutionary process of seamounts. U–Pb isotope dating is the most widely used method in current geochronology. However, the uranium content of carbonate minerals is typically two to four orders of magnitude lower than that of zircon, and common Pb is variable. Cheng et al. [21] and Kendrick et al. [22] presented an in situ U–Pb isotope dating method for low uranium content carbonate minerals using Laser Ablation Multi-Collector Inductively Coupled Plasma Mass Spectrometry (LA-MC-ICPMS) and developed a suitable carbonate mineral standard AHX-1a. This method allows for the quick and accurate determination of carbonate rock formation in seamounts. This study applies this method for conducting laser in situ U–Pb isotope dating of carbonate rock samples collected from Weijia Guyot (originally called Ita Mai Tai) in the Western Pacific Ocean. Research results provide chronological constraints for the island stage evolution of the seamount. They also provide an important basis for discussing the vertical evolution of the seamount.

The study area is located in Weijia Guyot, a feature of the Magellan Seamount Trail located in the Western Pacific Ocean (Figure 1). The Western Pacific Ocean is a region with a high concentration of seamounts due to its age and complex tectonic history. The formation of Weijia Guyot occurred between about 118 My and 120 My [23], which is associated with hotspot activity in the South Pacific Isotope and Thermal Anomalies Area (SOPITA) of the French Polynesian islands during the Cretaceous period [24–26]. Weijia Guyot is approximately 150 km long and has an irregular shape with an overall NE orientation, typical of a summit platform. The water depth at the edge of the platform ranges from 1600 m to 2200 m and reaches 5500 m at its base.

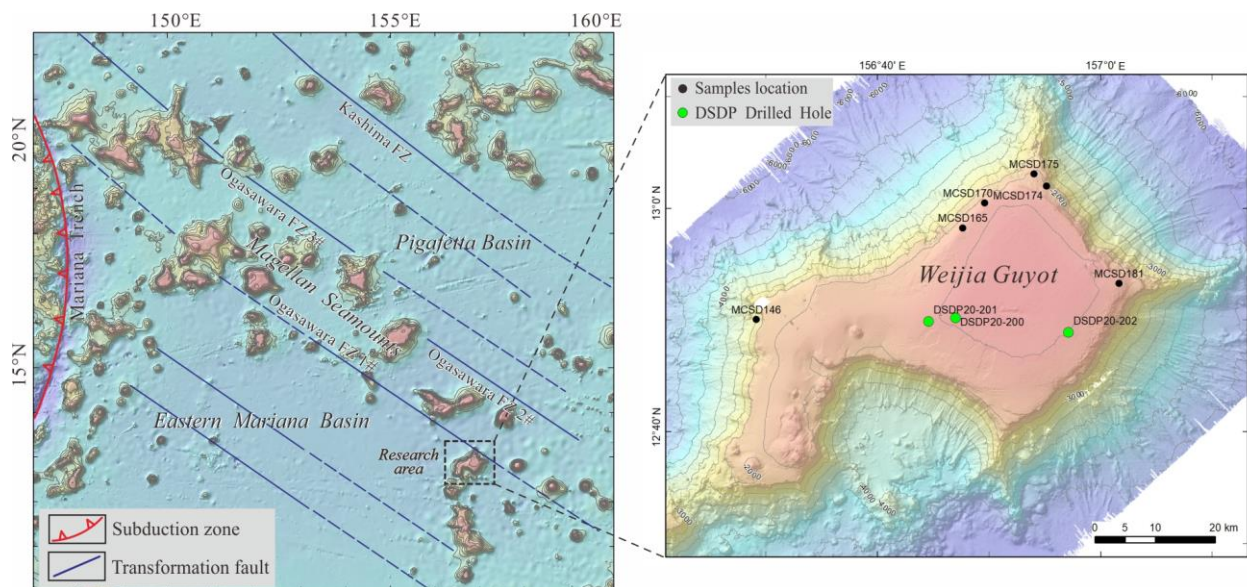


Figure 1. Structure sketch map of the Magellan seamounts and samples location.

2. Materials and Methods

2.1. The Studied Samples

Carbonate rock samples (Figure 2) were obtained by deep-sea shallow drilling at the edge of the platform or the slope of Weijia Guyot. The length of the cores ranges from 62 cm to 102 cm. These stations, including MCSD165, MCSD170, and MCSD181, are located at

the edge of the mountaintop platform with water depths ranging from 1594 m to 1630 m. MCSD174 and MCSD175 are located on a sloping platform with relatively flat terrain with water depths ranging from 1985 m to 2029 m. MCSD146 is located on steep slope areas with a water depth ranging from 2343 m to 2937 m (Figure 1).

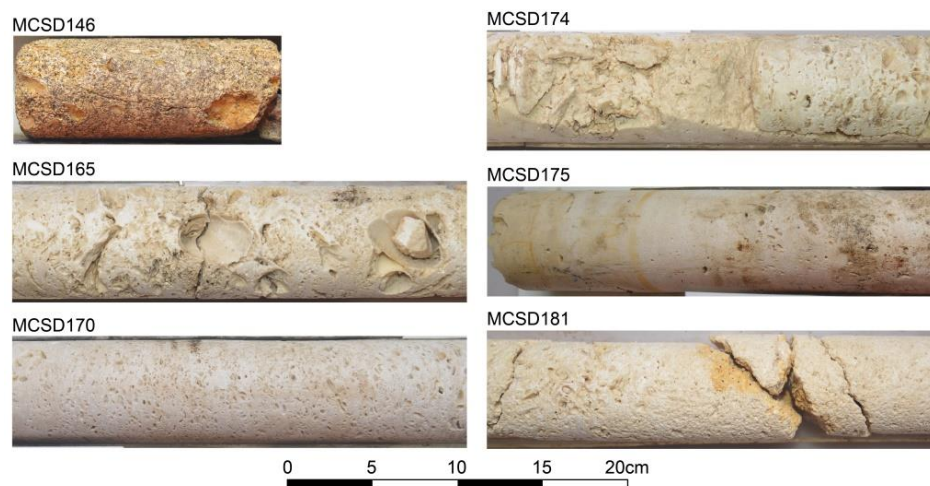


Figure 2. Photos of carbonate rock cores.

2.2. Microscopic Observation and Chemical Analysis

A polarizing microscope (Leica DM4 P, Leica Microsystems Inc., Deerfield, IL, USA) was used in this study to identify minerals in carbonate rock thin sections and capture micrographs. The MNR Key Laboratory of Marine Mineral Resources of GMGS conducted X-ray fluorescence analysis of major elements (XRF; Axios, PANalytical B.V., Almelo, The Netherlands), with a detection limit of 0.01–0.1% and a relative standard deviation (RSD) of less than 2%.

2.3. Laser In Situ U–Pb Isotope Dating

The samples were first sliced into 0.5 cm thick sections and carefully cleaned with water. Next, the clean part was selected, avoiding any parts mixed with clay or iron staining, to create circular sample targets with a diameter of 2.5 cm. The sample targets were then sanded, polished, and cleaned with anhydrous ethanol to avoid interference from common Pb [27].

Carbonate U–Pb dating was performed using laser ablation-multi-collector inductively coupled plasma-mass spectrometry (LA-MC-ICP-MS) employing a Nu Plasma II MC-ICP-MS coupled with a 193 nm ArF excimer laser system (RESOLUTION SE, ASI) at the Radiogenic Isotope Facility at the University of Queensland (Brisbane, Australia). The carbonate samples were screened using LA-ICP-MS (iCAP RQ, Thermo Scientific, Waltham, MA, USA) before U–Pb dating to confirm the laser spot position where the U/Pb ratio was highest and common Pb was lowest. To ensure accurate data, we tuned the instrument to glass standard NIST614 to reduce isotopic fractionation and oxidation levels before performing the experiments. The analysis began when the instrument signal was tuned to $^{206}\text{Pb}/^{238}\text{U} \approx 0.7$ and $\text{ThO}^+/\text{Th}^+ \approx 0.8\%$.

For laser ablation analyses, laser beams with diameters of 100 μm were used and set to a fluence of 2.5 J/cm^2 and a frequency of 10 Hz. Each analytical process began with 15 s, 20 s, and 15 s measurements for the background, sample ablation, and washout, respectively. Standard sample bracketing was used with NIST 614 glass as the primary reference material to correct $^{207}\text{Pb}/^{206}\text{Pb}$ fractionation and instrumental drift in $^{238}\text{U}/^{206}\text{Pb}$ ratios [28,29]. Carbonate reference AHX-1a (the recommended age is 209.8 ± 0.48 My) was used for the matrix-biased calibration of $^{238}\text{U}/^{206}\text{Pb}$ fractionation. Additionally, secondary reference material ASH15D (the recommended age is 2.965 ± 0.011 My) was used

to assess the accuracy of the dating results. During the experiment, three carbonate reference materials were inserted between each of the five analyses of unknown samples in measurement sequences. NIST614 was inserted every five spots throughout the whole sequence. Following the data reduction routine in Iolite v3 software [28], the calculated $^{207}\text{Pb}/^{206}\text{Pb}$ versus $^{238}\text{U}/^{206}\text{Pb}$ ratios were plotted in a Tera–Wasserburg diagram. The formation ages were determined from lower intercepts on inverse isochron using Isoplot 3.75 software in MS EXCEL [30].

3. Results

3.1. Microstructure and Mineral Characteristics of Carbonate Rocks

Based on field descriptions and microscopic analyses (Figure 3), carbonate rock grains mainly consist of carbonate bioclasts and coral reef clasts formed in a reef environment. MCS146 is a carbonate intraclast sandstone with a yellow color and high porosity. The rock grains consist of carbonate bioclasts, basalt clasts, palagonite clasts, and ooids, with bioclasts dominating. Basalt clasts, palagonite clasts, and ooids are dispersed in strips, with sparry calcite cementing the grains. MCS165, MCS170, MCS174, MCS175, and MCS181 are mineralogically similar, being pure white with a slight yellowish tinge. They are porous and consist mainly of carbonate bioclasts with some micritic limestone clasts. The cement is predominantly micritic, with some sparry calcite present.

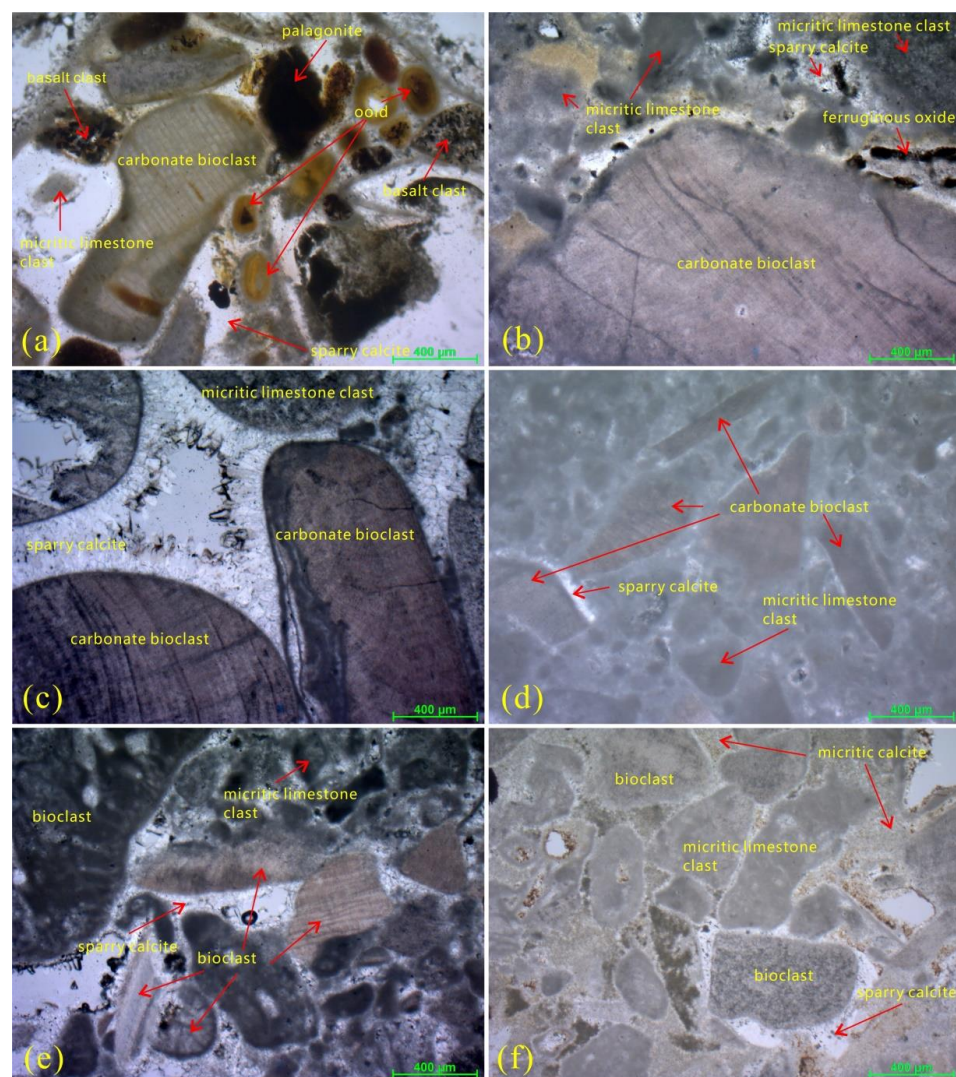


Figure 3. Micrographs of carbonate rocks (with plane polarized light). (a) MCS146; (b) MCS165; (c) MCS170; (d) MCS174; (e) MCS175; (f) MCS181.

3.2. Characteristics of Major Elements in Carbonate Rocks

Table 1 shows analysis results for major elements in carbonate rocks. All samples have a high loss on ignition (LOI), ranging from 29.95% to 43.41%. CaO content ranges from 40.08% to 56.37%; SiO₂ content ranges from 0.01% to 15.05%; Al₂O₃ content ranges from 0.01% to 6.11%, and Fe₂O₃ content ranges from 0 to 3.69%. MCSD146 contains basaltic clasts, so SiO₂, Al₂O₃, and Fe₂O₃ content are relatively high. The rest of the samples have high LOI with CaO content greater than 50%.

Table 1. Oxide content of major elements in carbonate rocks from Weijia Guyot (wt.%).

Samples	SiO ₂	Al ₂ O ₃	Fe ₂ O ₃	MgO	CaO	Na ₂ O	K ₂ O	MnO	TiO ₂	P ₂ O ₅	LOI	Total
MCSD146	15.05	6.11	3.69	0.72	40.08	1.31	1.30	0.11	0.92	1.32	29.95	100.56
MCSD165	0.08	0.02	0.01	0.51	55.67	0.33	0.01	0.01	0.02	3.35	40.21	100.21
MCSD170	0.01	0.01	0.01	0.61	56.08	0.25	0.01	0.00	0.02	0.02	43.29	100.29
MCSD174	0.03	0.05	0.00	0.66	55.74	0.22	0.01	0.00	0.03	0.09	43.41	100.23
MCSD175	0.01	0.01	0.00	0.61	55.77	0.26	0.01	0.01	0.03	0.42	43.40	100.52
MCSD181	1.70	0.06	0.05	0.46	56.37	0.43	0.02	0.00	0.02	0.84	39.66	99.61

3.3. Formation Age of Carbonate Rocks

Table A1 in Appendix A shows the U–Pb isotope dating analysis results for all carbonate rock samples. Table A2 lists the analysis results for standards AHS15D and AHX-1a. Figure A1 shows the Tera–Wasserburg concordia results for standards AHS15D and AHX-1a. The U content of carbonate rock samples is about two orders of magnitude lower than that of zircon and other uranium-rich minerals, ranging from 0.0102 to 6.5380 µg/g, with most of the analyzed points having a U content of less than 1 µg/g (accounting for 91%). On the contrary, although Pb content of samples is low, ranging from 0.0063–1.4320 µg/g, it is two to three orders of magnitude higher than that of zircon. This finding indicates a high level of common Pb content in the samples, which is difficult to subtract during data processing. Thus, the Tera–Wasserburg concordia diagram method, which does not require common Pb subtraction, was used to calculate U–Pb ages.

The Tera–Wasserburg concordia results (Figure 4) indicate that sample ages can be divided into two ranges: 91–96.8 My (MCSD165, MCSD174, and MCSD181) and 120–137 My (MCSD146, MCSD170, and MCSD175), suggesting that shallow-water carbonate rocks in the Weijia Guyot accumulated during two distinct events in the Early and Late Cretaceous periods respectively, with a hiatus of approximately 20 My.

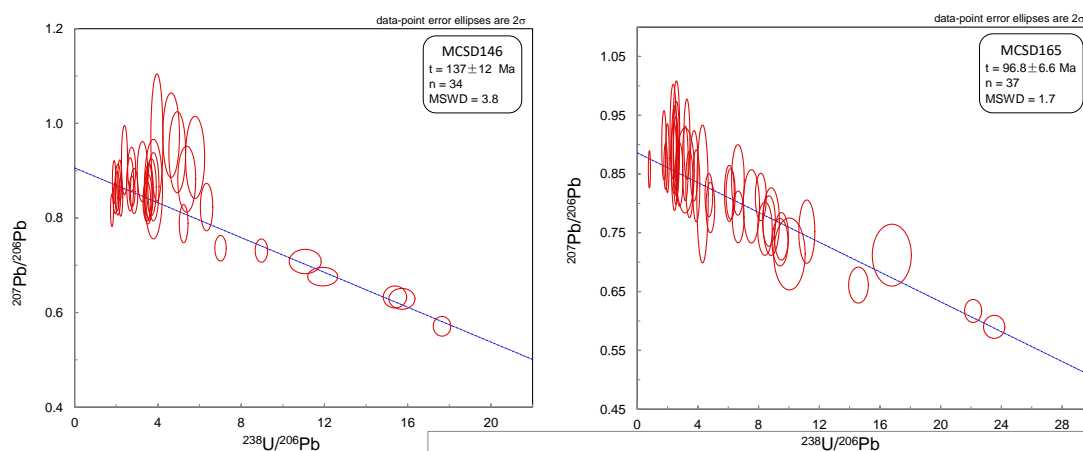


Figure 4. Cont.

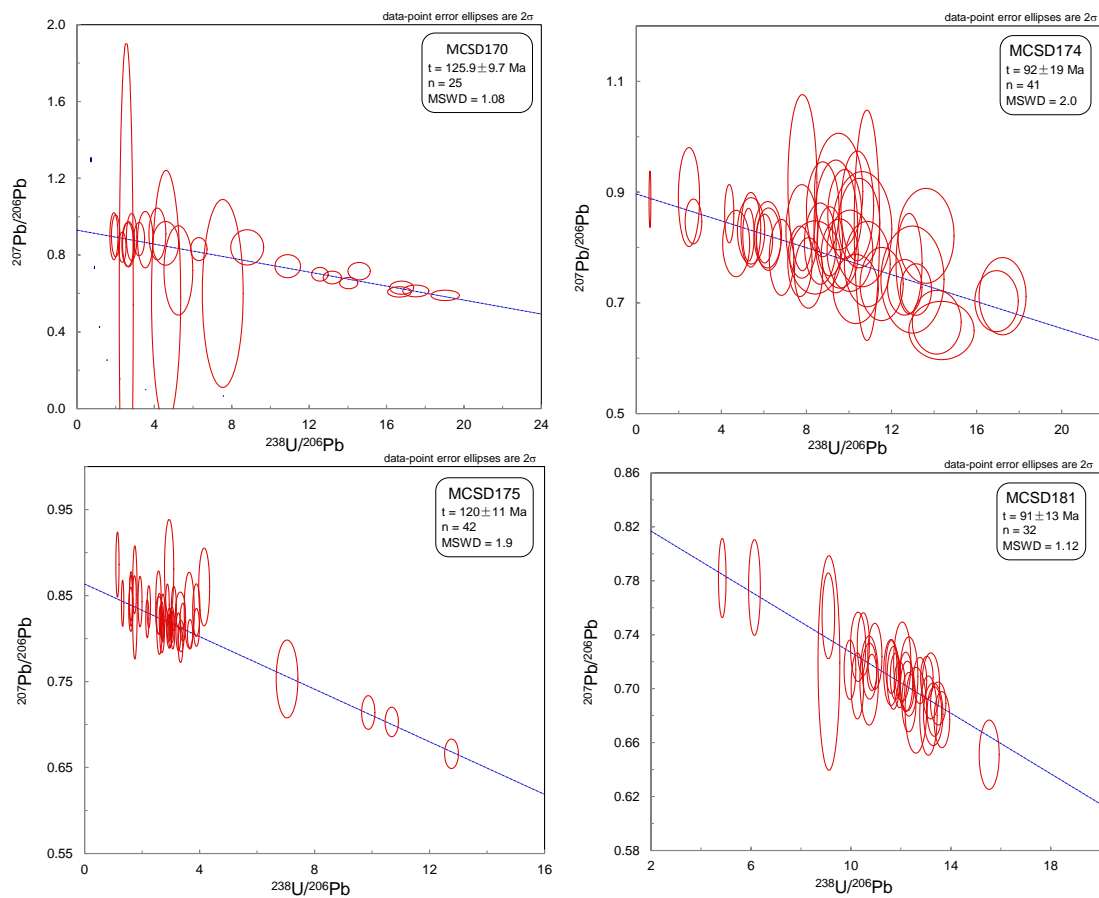


Figure 4. Laser in situ U–Pb isotope dating results of carbonate rocks.

4. Discussion

4.1. The Formation Time of the Initial Shield Volcano

According to analyses from ODP Sites 143 and 144, guyots in the Western Pacific Ocean are covered by Cretaceous shallow-water carbonate platforms [31]. After submergence, extinct seamounts remain intact until they are consumed by subduction or ocean basin closure [19]. The samples in this study showed no trace of undergoing late-stage alteration or metamorphism. The results of in situ U–Pb isotope dating represent the formation age of seamount carbonate rocks, which formed during the Hauterivian to Barremian and Cenomanian to Turonian ages.

The duration of volcanic activity on large seamounts can be substantial. Basalt samples from seamounts are prone to alteration due to prolonged seawater exposure. For these two reasons, the $^{40}\text{Ar}/^{39}\text{Ar}$ dating of seamount basalts is somewhat uncertain [5]. In addition, determining the main formation time of seamounts can be challenging due to the coverage of early shield-building basalt by younger alkaline lavas. Weijia Guyot evolved into its current form after multiple volcanic eruptions and underwent a long evolutionary process from shield volcanoes to its final stable stage. An age of 118–120 My ($^{40}\text{Ar}/^{39}\text{Ar}$) was obtained from the hawaiites of Weijia Guyot [26] and exhibited multiple late-stage small volcanic cones on its southwestern edge (Figure 1). According to U–Pb dating, the shallow-water carbonate cover of Weijia Guyot formed between 137 and 120 My, before the eruption of the hawaiites. Thus, the hawaiites at 118–120 My represent the seamount's subsequent activity. Due to uncertain dating, 10 My elapsed between the end of shield volcano-building and younger alkaline activity.

4.2. Genesis of the Second Stage Carbonate Rocks

The growth and demise of tropical carbonate platforms are influenced by numerous factors, including biota and skeletal particle production, sea level fluctuations, tectonic activity, volcanic eruptions, and environmental conditions [32]. The deposition of shallow-water carbonates on seamounts in the Northwestern Pacific Ocean was linked more closely with volcanic activities and tectonic movements [33]. Based on the dating results of shallow-water carbonate rocks, the Weijia Guyot entered the second stage of carbonate rock growth around 97 My (Cenomanian), approximately 20 My after the first stage of growth ceased. Weijia Guyot formed around 120 My in the South Pacific Isotope and Thermal Anomaly Zone (SOPITA) [24–26] and subsequently drifted northwestward with the Pacific Plate to its current location. According to Seton's global tectonic evolution model [34], Weijia Guyot was approximately 180 km away from the Society hotspot at 90 My [35]. Caiwei Guyot, located about 350 km northwest of Weijia Guyot, was also formed during the same period. During this period, there may have been multiple small-scale volcanic activities occurring in late stages at the southwestern edge of the seamount. Furthermore, it is postulated that the thermal uplift resulting from regional magmatic activity served as the principal factor responsible for the formation of the second stage shallow-water carbonate deposition in the Weijia Guyot.

5. Conclusions

(1) The results of laser in situ U–Pb isotope dating conducted on carbonate minerals reveal that the shallow-water carbonate rocks of the Weijia Guyot underwent two distinct formation phases: Hauterivian to Barremian followed by Cenomanian to Turonian, with a hiatus of approximately 20 My between them;

(2) Since the Hauterivian age (ca. 130 My), the shield volcano-building stage has been completed and exposed at or near the surface, allowing the deposition of the first carbonate platform. A temporal gap of approximately 10 My separates the cessation of shield volcanism and more recent alkaline volcanic activity;

(3) During the Turonian age (ca. 90 My), the regional tectonic uplift caused by the drift of the Weijia Guyot with the Pacific Plate toward the Society hotspot was the primary factor driving the formation of the second stage of shallow-water carbonate rocks.

Author Contributions: Conceptualization and methodology, Z.W. and J.M.; sample collection, Z.W., L.Z. (Limin Zhang) and B.Z.; formal analysis, Z.W., G.H. and J.M.; original draft preparation, Z.W. and L.Z. (Lifeng Zhong). All authors have read and agreed to the published version of the manuscript.

Funding: This research was funded by the National Natural Science Foundation of China, grant number 91958202, U2244222, 42176074, 42102111, and 42072324, and the Project from China Geological Survey, grant number 20221718 and 20230068.

Institutional Review Board Statement: Not applicable.

Informed Consent Statement: Not applicable.

Data Availability Statement: Data are available upon request from the author Z.W. (wei_zhenquan@163.com).

Acknowledgments: We are grateful to the onboard crew members of the cruise DY135-51 in the 2018 scientific expedition for sample collection.

Conflicts of Interest: The authors declare no conflict of interest.

Appendix A

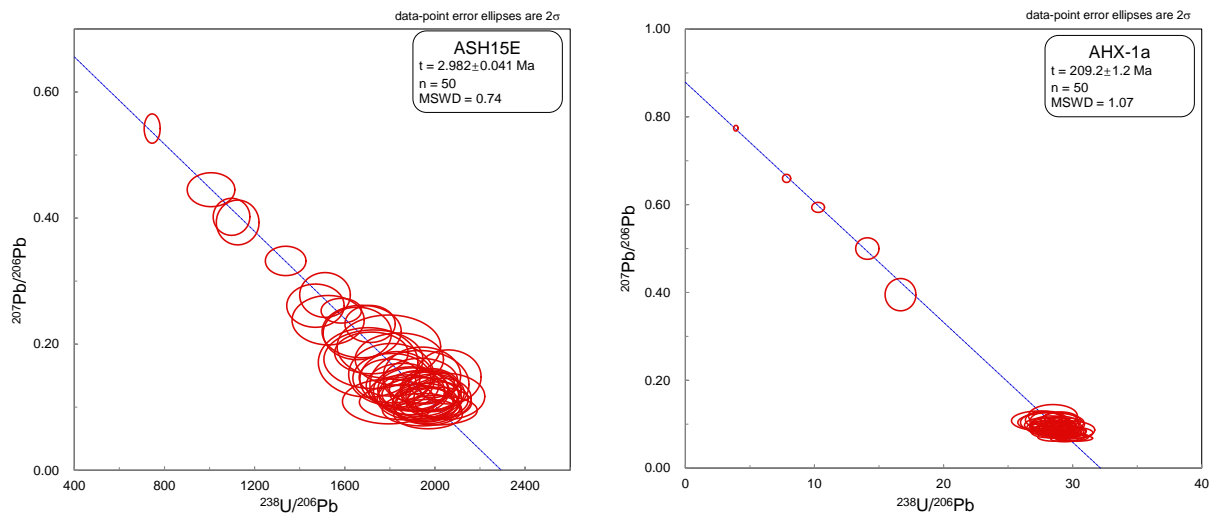


Figure A1. Laser in situ U-Pb isotope dating results for standards AHS15D and AHX-1a.

Table A1. U-Pb isotope analysis results of carbonate rocks.

Spot No.	U/ppm	Th/ppm	Pb/ppm	$^{238}\text{U}/^{206}\text{Pb}$	$\pm 2\sigma$	$^{207}\text{Pb}/^{206}\text{Pb}$	$\pm 2\sigma$	rho
MCSD146								
MCSD146-01	0.0546	0.0032	0.0660	3.9523	0.2376	0.9700	0.110	0.628
MCSD146-02	0.0567	0.0033	0.0553	2.8588	0.1469	0.8570	0.039	0.628
MCSD146-03	0.0537	0.0024	0.0473	1.9495	0.0788	0.8420	0.027	0.636
MCSD146-04	0.0477	0.0017	0.0303	2.3949	0.1190	0.9220	0.060	0.135
MCSD146-05	0.0653	0.0056	0.0420	5.3855	0.3529	0.8820	0.057	0.325
MCSD146-06	0.0480	0.0020	0.0295	8.9736	0.2449	0.7310	0.020	0.134
MCSD146-07	0.0597	0.0059	0.0322	2.2118	0.0812	0.8440	0.033	0.701
MCSD146-08	0.0722	0.0002	0.1090	5.7862	0.3749	0.9280	0.071	0.424
MCSD146-09	0.0755	0.0001	0.1048	3.2580	0.2055	0.8980	0.052	0.593
MCSD146-10	0.0524	0.0013	0.0671	4.6363	0.3269	0.9750	0.073	0.619
MCSD146-11	0.0787	0.0003	0.0943	2.1655	0.0778	0.8800	0.035	0.297
MCSD146-12	0.0488	0.0017	0.0522	5.2373	0.1707	0.7880	0.033	0.148
MCSD146-13	0.0677	0.0040	0.0718	2.7397	0.1557	0.9030	0.038	0.590
MCSD146-14	0.0541	0.0009	0.0422	1.8983	0.0698	0.8760	0.037	0.250
MCSD146-15	0.0619	0.0019	0.0455	3.6902	0.1883	0.8650	0.049	0.606
MCSD146-16	0.0541	0.0012	0.0324	2.6689	0.1379	0.8710	0.046	0.731
MCSD146-17	0.1602	0.0003	0.0784	17.6494	0.3445	0.5710	0.017	0.265
MCSD146-18	0.0535	0.0024	0.0247	2.0489	0.0813	0.8570	0.034	0.648
MCSD146-19	0.0563	0.0019	0.0246	11.0761	0.6276	0.7080	0.021	0.840
MCSD146-20	0.5780	0.0676	0.1494	3.4706	0.1515	0.8350	0.034	0.537
MCSD146-21	0.0673	0.0008	0.0996	3.5752	0.1272	0.8540	0.049	0.505
MCSD146-22	0.0721	0.0005	0.0995	15.3887	0.4584	0.6330	0.019	0.544
MCSD146-23	0.1514	0.0003	0.1545	1.7947	0.0579	0.8160	0.028	0.502
MCSD146-24	0.0996	0.0001	0.0807	3.5247	0.1649	0.8400	0.043	0.532
MCSD146-25	0.0614	0.0001	0.0436	7.0084	0.2241	0.7360	0.022	0.287
MCSD146-26	0.0576	0.0001	0.0433	2.7606	0.1159	0.8560	0.026	0.709
MCSD146-27	0.0880	0.0000	0.0675	15.7233	0.5127	0.6290	0.018	0.251
MCSD146-28	0.1115	0.0001	0.0461	3.5629	0.1755	0.8570	0.047	0.213
MCSD146-29	0.2345	0.0592	0.0769	6.3389	0.2444	0.8230	0.041	0.573
MCSD146-30	0.5380	0.0579	0.1121	11.9155	0.5889	0.6760	0.016	0.217
MCSD146-31	0.9886	0.1210	0.1789	3.7868	0.2181	0.8660	0.059	0.119
MCSD146-32	0.7841	0.0848	0.1032	4.9303	0.3294	0.9390	0.070	0.314
MCSD146-33	1.3045	0.1752	0.1660	3.7868	0.3569	0.8610	0.086	0.250
MCSD146-34	0.9920	0.1004	0.1005	2.0784	0.1194	0.8600	0.044	0.276

Table A1. Cont.

Spot No.	U/ppm	Th/ppm	Pb/ppm	²³⁸ U/ ²⁰⁶ Pb	±2σ	²⁰⁷ Pb/ ²⁰⁶ Pb	±2σ	rho
MCSD165								
MCSD165-01	0.3230	0.0001	0.1265	6.1555	0.2462	0.8160	0.035	0.215
MCSD165-02	0.2442	0.0003	0.0947	6.6355	0.3409	0.8400	0.049	0.284
MCSD165-03	0.2909	0.0002	0.1073	6.6538	0.3183	0.7770	0.036	0.356
MCSD165-04	0.2940	0.0002	0.0985	7.5262	0.4386	0.7950	0.051	0.386
MCSD165-05	0.4333	0.0000	0.1349	8.1449	0.2935	0.8110	0.033	0.101
MCSD165-06	0.3941	0.0001	0.1030	8.6827	0.3440	0.7700	0.035	0.646
MCSD165-07	0.3782	0.0001	0.1013	8.8311	0.4421	0.7690	0.047	0.707
MCSD165-08	0.4465	0.0005	0.1114	9.4176	0.4292	0.7340	0.033	0.357
MCSD165-09	0.4519	0.0032	0.1058	9.5042	0.3747	0.7440	0.033	0.212
MCSD165-10	0.4980	0.0001	0.1024	10.0315	0.8487	0.7140	0.050	0.351
MCSD165-11	1.1500	0.0034	0.1557	14.5821	0.5292	0.6610	0.025	0.312
MCSD165-12	2.0060	0.0035	0.2470	16.7812	1.0513	0.7120	0.043	0.157
MCSD165-13	4.9170	0.0087	0.4312	22.1387	0.4608	0.6170	0.016	0.130
MCSD165-14	4.3540	0.0120	0.3459	23.5286	0.5741	0.5900	0.016	0.517
MCSD165-15	0.0724	0.0009	0.2360	0.8027	0.0561	0.8580	0.026	0.407
MCSD165-16	0.1215	0.0001	0.1786	1.8738	0.0971	0.8630	0.032	0.544
MCSD165-17	0.0662	0.0002	0.0683	2.4190	0.1537	0.8770	0.049	0.598
MCSD165-18	0.0724	0.0003	0.0714	2.4601	0.1757	0.8770	0.073	0.248
MCSD165-19	0.0748	0.0002	0.0721	2.5831	0.1661	0.8930	0.066	0.472
MCSD165-20	0.0750	0.0002	0.0771	2.5831	0.1753	0.9230	0.070	0.207
MCSD165-21	0.0794	0.0003	0.0770	2.7926	0.1833	0.8490	0.044	0.483
MCSD165-22	0.0703	0.0002	0.0650	3.7475	0.2136	0.8640	0.049	0.811
MCSD165-23	0.1197	0.0003	0.0817	4.7211	0.2065	0.8140	0.030	0.622
MCSD165-24	0.2710	0.0003	0.1424	4.8218	0.2347	0.7930	0.035	0.536
MCSD165-25	0.2249	0.0000	0.1159	8.4199	0.3921	0.7570	0.037	0.612
MCSD165-26	0.3329	0.0002	0.0902	11.1788	0.4319	0.7520	0.044	0.685
MCSD165-27	0.5820	0.0002	0.1153	1.7641	0.1205	0.8990	0.048	0.518
MCSD165-28	0.4904	0.0009	0.0932	1.9870	0.0983	0.8770	0.048	0.244
MCSD165-29	0.0629	0.0004	0.1195	2.3714	0.1711	0.9220	0.066	0.249
MCSD165-30	0.0675	0.0005	0.1096	2.5467	0.1435	0.8730	0.061	0.377
MCSD165-31	0.0758	0.0000	0.0980	3.1584	0.4965	0.8560	0.059	0.132
MCSD165-32	0.0766	0.0002	0.0821	3.1722	0.1530	0.8680	0.052	0.147
MCSD165-33	0.0834	0.0003	0.0808	3.2727	0.1629	0.9090	0.056	0.187
MCSD165-34	0.0991	0.0003	0.0710	3.4441	0.1968	0.8320	0.046	0.439
MCSD165-35	0.0962	0.0002	0.0801	3.8886	0.1944	0.8300	0.050	0.264
MCSD165-36	0.1004	0.0003	0.0819	4.3052	0.3075	0.8160	0.096	0.232
MCSD165-37	0.1041	0.0002	0.0744	6.0728	0.2651	0.8170	0.039	0.550
MCSD170								
MCSD170-01	0.0196	0.0000	0.0215	2.6689	0.2561	0.8560	0.096	0.557
MCSD170-02	0.0102	0.0000	0.0092	3.2145	0.2286	0.8830	0.071	0.959
MCSD170-03	0.0153	0.0000	0.0118	4.1567	0.3583	0.9100	0.110	0.461
MCSD170-04	0.0133	0.0000	0.0111	3.5281	0.3270	0.8800	0.120	0.968
MCSD170-05	0.0236	0.0001	0.0216	2.8253	0.2207	0.8940	0.100	0.243
MCSD170-06	0.0106	0.0000	0.0063	2.3407	0.1591	0.8410	0.064	0.972
MCSD170-07	0.0339	0.0000	0.0290	2.5467	0.2959	0.5400	1.120	0.613
MCSD170-08	0.0128	0.0000	0.0096	4.5777	0.5505	0.8610	0.093	0.976
MCSD170-09	0.0154	0.0000	0.0095	8.7989	0.6958	0.8400	0.075	0.244
MCSD170-10	0.0236	0.0000	0.0123	12.5568	0.3488	0.7000	0.029	0.386
MCSD170-11	0.0152	0.0000	0.0070	14.0441	0.3818	0.6754	0.024	0.910
MCSD170-12	0.0181	0.0000	0.0066	16.6652	0.4992	0.6080	0.022	0.279
MCSD170-13	0.0281	0.0000	0.0141	17.5126	0.5512	0.6130	0.025	0.611
MCSD170-14	0.1069	0.0008	0.0430	16.7812	0.5062	0.6300	0.028	0.526
MCSD170-15	0.0534	0.0000	0.0130	10.8926	0.5414	0.7420	0.049	0.683
MCSD170-16	0.1430	0.0004	0.0316	13.1984	0.3854	0.6830	0.027	0.820
MCSD170-17	0.4637	0.0020	0.0807	6.3003	0.3457	0.8310	0.049	0.575
MCSD170-18	0.5930	0.0105	0.1016	19.0334	0.6011	0.5900	0.022	0.604
MCSD170-19	0.6472	0.0025	0.0976	14.5821	0.4704	0.7160	0.037	0.429
MCSD170-20	0.4957	0.0017	0.0758	1.9084	0.1712	0.8980	0.100	0.350

Table A1. Cont.

Spot No.	U/ppm	Th/ppm	Pb/ppm	²³⁸ U/ ²⁰⁶ Pb	±2σ	²⁰⁷ Pb/ ²⁰⁶ Pb	±2σ	rho
MCSD170-21	0.7112	0.0029	0.0790	2.6205	0.2469	0.8550	0.094	0.667
MCSD170-22	0.8100	0.0039	0.0950	4.6068	0.6162	0.5800	0.540	0.768
MCSD170-23	0.6045	0.0025	0.0750	5.2411	0.6077	0.7200	0.190	0.674
MCSD170-24	0.6830	0.0036	0.0763	7.5341	0.8633	0.6000	0.400	0.719
MCSD170-25	0.7925	0.0027	0.0801	1.9980	0.1766	0.9005	0.089	0.687
MCSD174								
MCSD174-01	0.0854	0.0043	0.0507	11.5354	0.8279	0.7340	0.054	0.410
MCSD174-02	0.0835	0.0001	0.0411	5.2755	0.2193	0.8230	0.039	0.669
MCSD174-03	0.0500	0.0000	0.0167	7.6944	0.4666	0.7750	0.052	0.300
MCSD174-04	0.0670	0.0021	0.0195	8.0993	0.5442	0.7540	0.052	0.488
MCSD174-05	0.0528	0.0000	0.0161	8.7669	0.6270	0.8690	0.070	0.236
MCSD174-06	0.0578	0.0000	0.0156	9.3809	0.8395	0.8380	0.098	0.409
MCSD174-07	0.0644	0.0000	0.0165	10.3918	0.6271	0.8750	0.081	0.830
MCSD174-08	0.0551	0.0000	0.0144	10.8599	0.8805	0.7700	0.063	0.660
MCSD174-09	0.0859	0.0000	0.0223	9.0977	0.4921	0.8110	0.051	0.452
MCSD174-10	0.0531	0.0000	0.0148	6.8297	0.4708	0.7820	0.056	0.532
MCSD174-11	0.0600	0.0000	0.0194	10.3177	0.8684	0.7250	0.051	0.916
MCSD174-12	0.0776	0.0001	0.0184	8.6516	0.6106	0.8070	0.060	0.645
MCSD174-13	0.0763	0.0000	0.0141	4.3702	0.1769	0.8610	0.043	0.495
MCSD174-14	0.0782	0.0000	0.0134	10.6207	1.1385	0.8330	0.085	0.204
MCSD174-15	0.0126	0.0069	0.0531	9.5167	0.9266	0.9010	0.086	0.681
MCSD174-16	0.0863	0.0000	0.0356	7.8107	0.5567	0.9170	0.130	0.552
MCSD174-17	0.0883	0.0001	0.0264	6.0323	0.3119	0.8160	0.036	0.482
MCSD174-18	0.0780	0.0001	0.0201	9.8004	0.6507	0.8600	0.066	0.490
MCSD174-19	0.0994	0.0002	0.0209	10.8436	0.4877	0.8400	0.170	0.539
MCSD174-20	0.1093	0.0000	0.0216	12.8239	0.5002	0.7710	0.074	0.706
MCSD174-21	0.1402	0.0000	0.0232	14.1264	0.9381	0.6650	0.047	0.625
MCSD174-22	0.1485	0.0000	0.0265	16.9384	0.8330	0.7030	0.045	0.467
MCSD174-23	0.1429	0.0000	0.0233	14.3506	1.2528	0.6500	0.043	0.717
MCSD174-24	0.1178	0.0000	0.0161	13.1504	0.5977	0.7240	0.038	0.667
MCSD174-25	0.1427	0.0000	0.0188	0.6435	0.0355	0.8870	0.042	0.286
MCSD174-26	0.1453	0.0000	0.0158	12.6225	0.6609	0.7280	0.041	0.506
MCSD174-27	0.1352	0.0000	0.0148	17.2207	0.9020	0.7120	0.057	0.098
MCSD174-28	0.1326	0.0000	0.0128	10.0454	0.8790	0.7940	0.060	0.202
MCSD174-29	0.0735	0.0003	0.0810	8.4101	0.9779	0.7820	0.054	0.518
MCSD174-30	0.0758	0.0002	0.0920	2.4770	0.4072	0.8910	0.073	0.465
MCSD174-31	0.0699	0.0003	0.0386	4.6966	0.5185	0.8070	0.049	0.638
MCSD174-32	0.0648	0.0001	0.0281	5.3975	0.5236	0.8300	0.049	0.600
MCSD174-33	0.0672	0.0001	0.0333	6.2137	0.4751	0.8150	0.046	0.523
MCSD174-34	0.0664	0.0001	0.0263	9.5671	0.7087	0.7890	0.051	0.667
MCSD174-35	0.0689	0.0000	0.0281	10.4822	0.7900	0.8440	0.066	0.389
MCSD174-36	0.0817	0.0001	0.0249	12.9851	1.2123	0.7420	0.079	0.580
MCSD174-37	0.0839	0.0000	0.0186	7.7855	0.6118	0.8290	0.069	0.585
MCSD174-38	0.0865	0.0000	0.0179	6.1818	0.5284	0.8230	0.049	0.653
MCSD174-39	0.0800	0.0001	0.0195	5.3855	0.3810	0.8320	0.055	0.538
MCSD174-40	0.0831	0.0000	0.0150	2.6887	0.3198	0.8470	0.033	0.545
MCSD174-41	0.0899	0.0000	0.0125	13.6209	1.0774	0.8210	0.070	0.755
MCSD175								
MCSD175-01	0.1471	0.0042	0.2504	1.6181	0.0507	0.8460	0.026	0.413
MCSD175-02	0.0946	0.0129	0.1629	2.2330	0.0483	0.8370	0.020	0.707
MCSD175-03	0.1417	0.0036	0.1949	2.5868	0.0916	0.8270	0.018	0.696
MCSD175-04	0.2016	0.0065	0.2461	2.8793	0.0527	0.8390	0.020	0.542
MCSD175-05	0.2876	0.0075	0.3290	2.9740	0.0391	0.8040	0.012	0.274
MCSD175-06	0.2852	0.0042	0.2982	3.0686	0.0586	0.8100	0.018	0.450
MCSD175-07	0.1066	0.0046	0.1064	7.0426	0.3086	0.7530	0.037	0.677
MCSD175-08	0.2451	0.0039	0.2327	2.6045	0.0816	0.8170	0.029	0.603
MCSD175-09	0.5497	0.0110	0.5171	3.0402	0.0613	0.8160	0.017	0.572
MCSD175-10	0.8930	0.0102	0.7990	1.9287	0.0566	0.8430	0.024	0.567
MCSD175-11	0.3633	0.0116	0.3188	1.6073	0.0607	0.8340	0.021	0.642
MCSD175-12	0.3175	0.0085	0.2751	2.9235	0.0414	0.8120	0.013	0.687

Table A1. Cont.

Spot No.	U/ppm	Th/ppm	Pb/ppm	²³⁸ U/ ²⁰⁶ Pb	±2σ	²⁰⁷ Pb/ ²⁰⁶ Pb	±2σ	rho
MCSD175-13	0.5324	0.0152	0.4239	3.3516	0.0870	0.8030	0.015	0.325
MCSD175-14	0.1906	0.0011	0.0631	2.5712	0.0777	0.8420	0.030	0.428
MCSD175-15	0.1444	0.0065	0.3013	1.3222	0.0338	0.8410	0.022	0.402
MCSD175-16	0.2320	0.0062	0.2880	2.6339	0.0326	0.8220	0.013	0.551
MCSD175-17	0.6273	0.0177	0.6570	2.7221	0.0420	0.8130	0.014	0.208
MCSD175-18	0.2821	0.0071	0.2898	2.9509	0.0819	0.8120	0.019	0.560
MCSD175-19	0.5510	0.0161	0.5484	3.1042	0.0719	0.8350	0.021	0.607
MCSD175-20	0.0775	0.0002	0.0726	3.3315	0.1396	0.8320	0.018	0.349
MCSD175-21	0.3480	0.0057	0.3340	3.6696	0.0745	0.8050	0.014	0.199
MCSD175-22	0.7650	0.0099	0.6850	3.4181	0.0808	0.8190	0.018	0.332
MCSD175-23	0.3331	0.0066	0.2882	2.1805	0.0434	0.8230	0.018	0.490
MCSD175-24	0.4231	0.0122	0.3515	3.2639	0.0692	0.8080	0.018	0.322
MCSD175-25	0.3159	0.0055	0.2472	3.8865	0.1044	0.8330	0.025	0.435
MCSD175-26	0.4018	0.0055	0.3091	2.9401	0.1315	0.8810	0.047	0.385
MCSD175-27	0.6650	0.0086	0.4919	3.0262	0.0418	0.8170	0.012	0.472
MCSD175-28	0.3371	0.0070	0.2372	2.6867	0.0529	0.8210	0.018	0.144
MCSD175-29	0.0583	0.0006	0.1453	1.1426	0.0451	0.8860	0.031	0.408
MCSD175-30	0.1098	0.0078	0.1875	1.7345	0.0499	0.8510	0.018	0.574
MCSD175-31	0.2481	0.0066	0.3937	2.6927	0.0602	0.8020	0.015	0.559
MCSD175-32	0.1119	0.0024	0.1823	2.9789	0.0405	0.8150	0.011	0.425
MCSD175-33	0.2978	0.0097	0.2990	3.6382	0.1427	0.8330	0.036	0.426
MCSD175-34	0.1841	0.0044	0.1906	4.1591	0.1555	0.8600	0.037	0.423
MCSD175-35	0.7029	0.0095	0.6481	12.7628	0.1959	0.6660	0.014	0.463
MCSD175-36	0.3670	0.0039	0.3037	1.7470	0.0675	0.8420	0.054	0.545
MCSD175-37	0.0891	0.0019	0.0639	9.8673	0.1885	0.7140	0.016	0.683
MCSD175-38	0.5467	0.0088	0.3768	3.8906	0.0837	0.8130	0.018	0.306
MCSD175-39	0.1318	0.0020	0.0866	1.6108	0.0431	0.8470	0.022	0.444
MCSD175-40	1.0307	0.0057	0.2473	10.6835	0.1894	0.7030	0.014	0.375
MCSD175-41	1.1504	0.0079	0.2540	3.3361	0.0662	0.7930	0.017	0.483
MCSD175-42	1.8770	0.0134	0.3251	2.7262	0.0586	0.8260	0.021	0.674
MCSD181								
MCSD181-01	0.2685	0.0062	0.1442	6.1398	0.1928	0.7750	0.029	0.434
MCSD181-02	0.2950	0.0106	0.1221	10.4974	0.1981	0.7330	0.019	0.574
MCSD181-03	0.4159	0.0087	0.1216	10.7470	0.2395	0.7130	0.017	0.349
MCSD181-04	0.5379	0.0933	0.1506	10.9586	0.2325	0.7240	0.020	0.276
MCSD181-05	0.8900	0.0307	0.2121	12.2588	0.2286	0.7020	0.015	0.498
MCSD181-06	0.8620	0.0390	0.2000	12.7651	0.2185	0.7060	0.014	0.031
MCSD181-07	0.8700	0.0155	0.1887	10.7310	0.3025	0.7060	0.027	0.583
MCSD181-08	1.1550	0.0238	0.2430	11.6095	0.2423	0.7120	0.020	0.354
MCSD181-09	1.0100	0.0220	0.2091	11.7034	0.2083	0.7080	0.019	0.515
MCSD181-10	1.5520	0.0396	0.2987	9.0977	0.2060	0.7540	0.026	0.783
MCSD181-11	1.5140	0.0888	0.2954	4.8509	0.1236	0.7820	0.024	0.276
MCSD181-12	1.7550	0.0593	0.3271	12.3215	0.2309	0.6900	0.018	0.625
MCSD181-13	0.8969	0.0170	0.1402	9.1207	0.3565	0.7190	0.065	0.622
MCSD181-14	1.7470	0.0193	0.2225	10.2592	0.2037	0.7020	0.020	0.403
MCSD181-15	0.8195	0.0026	0.2150	13.2954	0.3177	0.6810	0.019	0.584
MCSD181-16	0.4932	0.0175	0.1251	15.5342	0.3270	0.6510	0.021	0.097
MCSD181-17	0.6345	0.0327	0.1472	13.0389	0.2045	0.7080	0.013	0.684
MCSD181-18	1.1340	0.0016	0.2474	9.9624	0.1921	0.7140	0.018	0.191
MCSD181-19	1.3460	0.0310	0.2535	13.3420	0.2363	0.6830	0.015	0.493
MCSD181-20	0.8130	0.0326	0.1406	12.1968	0.2262	0.7050	0.018	0.413
MCSD181-21	2.1250	0.0320	0.3827	12.6005	0.3512	0.6840	0.026	0.233
MCSD181-22	0.9380	0.0223	0.1591	13.6440	0.2548	0.6770	0.017	0.561
MCSD181-23	1.9550	0.0272	0.3330	11.6188	0.1829	0.7160	0.016	0.258
MCSD181-24	1.8320	0.0315	0.2997	11.7835	0.1689	0.7090	0.014	0.327
MCSD181-25	1.2570	0.0007	0.1630	12.0545	0.2813	0.7200	0.024	0.563
MCSD181-26	1.5810	0.0231	0.2136	12.3215	0.2939	0.7090	0.024	0.082
MCSD181-27	0.8300	0.0512	0.1912	13.1027	0.2848	0.6800	0.024	0.313

Table A1. Cont.

Spot No.	U/ppm	Th/ppm	Pb/ppm	²³⁸ U/ ²⁰⁶ Pb	±2σ	²⁰⁷ Pb/ ²⁰⁶ Pb	±2σ	rho
MCSD181-28	6.5380	0.0220	1.4320	13.4939	0.2518	0.6890	0.013	0.152
MCSD181-29	2.1140	0.0331	0.4297	13.1984	0.2890	0.7020	0.020	0.282
MCSD181-30	5.8600	0.0206	1.1900	10.8404	0.1544	0.7120	0.011	0.063
MCSD181-31	5.3200	0.0187	1.0970	10.2883	0.2488	0.7310	0.021	0.174
MCSD181-32	3.4900	0.0206	0.7060	11.9490	0.1757	0.7030	0.014	0.558

Table A2. U–Pb isotope analysis results for standards AHS15D and AHX-1a.

	U/ppm	Th/ppm	Pb/ppm	²³⁸ U/ ²⁰⁶ Pb	±2σ	²⁰⁷ Pb/ ²⁰⁶ Pb	±2σ	rho
ASH15D								
ASH15D_1	1.6070	0.0000	0.0011	1526.270	130.890	0.238	0.032	−0.614
ASH15D_2	3.2510	0.0000	0.0021	1584.505	73.054	0.253	0.016	−0.483
ASH15D_3	2.7730	0.0000	0.0007	1935.251	139.037	0.120	0.022	−0.690
ASH15D_4	3.4200	0.0000	0.0007	1942.795	143.911	0.096	0.021	−0.835
ASH15D_5	3.0820	0.0000	0.0006	1958.063	103.866	0.107	0.021	−0.755
ASH15D_6	1.5070	0.0000	0.0012	1469.991	104.070	0.261	0.028	−0.526
ASH15D_7	2.2960	0.0000	0.0007	1902.011	127.043	0.128	0.028	−0.718
ASH15D_8	2.1450	0.0000	0.0004	1876.938	137.854	0.123	0.023	−0.674
ASH15D_9	2.7710	0.0000	0.0016	1655.572	123.755	0.217	0.034	−0.796
ASH15D_10	2.2490	0.0000	0.0014	1727.303	179.616	0.176	0.038	−0.776
ASH15D_11	3.5910	0.0000	0.0007	2013.442	109.824	0.112	0.023	−0.797
ASH15D_12	2.7990	0.0000	0.0010	1799.014	110.409	0.147	0.024	−0.820
ASH15D_13	3.5240	0.0000	0.0020	1718.369	133.322	0.186	0.027	−0.861
ASH15D_14	1.8960	0.0000	0.0030	1124.891	77.447	0.393	0.029	−0.285
ASH15D_15	1.9400	0.0000	0.0004	1969.672	124.564	0.089	0.019	−0.410
ASH15D_16	1.8490	0.0000	0.0004	1981.420	110.298	0.127	0.028	−0.550
ASH15D_17	1.8951	0.0000	0.0040	1006.721	86.436	0.445	0.022	−0.642
ASH15D_18	1.7510	0.0000	0.0009	1795.773	187.666	0.196	0.041	−0.714
ASH15D_19	1.6230	0.0000	0.0006	1942.795	140.124	0.150	0.037	−0.559
ASH15D_20	1.9000	0.0000	0.0007	1805.532	153.732	0.152	0.040	−0.752
ASH15D_21	2.0850	0.0000	0.0007	1842.244	160.047	0.176	0.034	−0.685
ASH15D_22	2.2200	0.0000	0.0038	1097.637	66.487	0.402	0.024	−0.360
ASH15D_23	2.1943	0.0000	0.0004	1931.499	153.472	0.113	0.028	−0.681
ASH15D_24	0.9430	0.0000	0.0003	1931.499	179.674	0.136	0.044	−0.426
ASH15D_25	2.2390	0.0000	0.0019	1512.373	91.798	0.278	0.029	−0.555
ASH15D_26	2.1350	0.0000	0.0071	745.441	28.992	0.542	0.019	−0.106
ASH15D_27	3.1410	0.0000	0.0034	1337.791	73.623	0.332	0.019	−0.533
ASH15D_28	2.2800	0.0000	0.0011	1712.464	91.214	0.232	0.024	−0.322
ASH15D_29	2.0800	0.0000	0.0004	2033.987	103.775	0.114	0.026	−0.500
ASH15D_30	3.0580	0.0002	0.0006	1958.063	119.253	0.107	0.025	−0.653
ASH15D_31	1.9590	0.0000	0.0003	1965.787	120.196	0.102	0.023	−0.559
ASH15D_32	2.5280	0.0000	0.0009	1795.773	168.253	0.109	0.029	−0.804
ASH15D_33	2.1500	0.0000	0.0005	1946.590	110.256	0.105	0.023	−0.579
ASH15D_34	2.2170	0.0000	0.0006	1920.335	99.902	0.126	0.026	−0.665
ASH15D_35	1.6890	0.0000	0.0008	1703.682	180.561	0.171	0.045	−0.775
ASH15D_36	2.9710	0.0000	0.0006	1989.329	115.151	0.123	0.024	−0.700
ASH15D_37	3.9880	0.0000	0.0008	2017.518	118.437	0.107	0.020	−0.697
ASH15D_38	3.3240	0.0000	0.0010	1876.938	173.201	0.108	0.023	−0.816
ASH15D_39	3.1670	0.0000	0.0007	1985.367	106.783	0.126	0.025	−0.680
ASH15D_40	1.6260	0.0000	0.0004	1927.764	145.421	0.121	0.029	−0.484
ASH15D_41	1.1290	0.0000	0.0007	1675.048	143.576	0.220	0.034	−0.196
ASH15D_42	4.4900	0.0000	0.0010	1985.367	83.053	0.137	0.018	−0.630
ASH15D_43	1.6030	0.0000	0.0004	1894.780	136.885	0.126	0.031	−0.463
ASH15D_44	3.6600	0.0000	0.0012	1855.966	131.335	0.134	0.029	−0.839
ASH15D_45	1.7330	0.0000	0.0004	1935.251	135.280	0.142	0.029	−0.426
ASH15D_46	3.6880	0.0000	0.0007	2005.339	149.291	0.095	0.019	−0.760
ASH15D_47	1.5720	0.0000	0.0004	2059.203	119.127	0.148	0.035	−0.547

Table A2. Cont.

	U/ppm	Th/ppm	Pb/ppm	²³⁸ U/ ²⁰⁶ Pb	±2σ	²⁰⁷ Pb/ ²⁰⁶ Pb	±2σ	rho
ASH15D_48	1.6580	0.0000	0.0004	2046.517	142.878	0.117	0.030	−0.542
ASH15D_49	1.4320	0.0000	0.0005	1832.084	134.712	0.144	0.036	−0.551
ASH15D_50	1.8590	0.0000	0.0007	1808.809	141.159	0.146	0.032	−0.704
AHX-1a								
AHX-1a_1	0.1387	0.0000	0.0015	28.314	1.287	0.098	0.017	−0.847
AHX-1a_2	0.0982	0.0001	0.0008	28.998	1.012	0.098	0.009	−0.707
AHX-1a_3	0.1408	0.0001	0.0017	29.662	1.677	0.087	0.017	−0.881
AHX-1a_4	0.1079	0.0001	0.0005	29.733	0.976	0.070	0.007	−0.310
AHX-1a_5	0.1291	0.0000	0.0019	28.314	2.091	0.104	0.018	−0.868
AHX-1a_6	0.0930	0.0001	0.0006	29.091	1.019	0.092	0.012	−0.696
AHX-1a_7	0.1345	0.0001	0.1227	3.913	0.143	0.774	0.005	−0.295
AHX-1a_8	0.0929	0.0001	0.0007	28.872	1.004	0.092	0.012	−0.646
AHX-1a_9	0.1264	0.0003	0.0146	16.666	0.975	0.395	0.030	−0.925
AHX-1a_10	0.1000	0.0003	0.0005	29.253	1.030	0.077	0.007	−0.650
AHX-1a_11	0.1261	0.0002	0.0015	28.939	1.008	0.097	0.014	−0.804
AHX-1a_12	0.1032	0.0001	0.0011	27.996	1.258	0.092	0.013	−0.784
AHX-1a_13	0.1188	0.0001	0.0007	30.330	1.015	0.080	0.010	−0.471
AHX-1a_14	0.1012	0.0001	0.0006	29.210	0.942	0.081	0.010	−0.676
AHX-1a_15	0.1058	0.0001	0.0009	28.395	1.294	0.095	0.011	−0.749
AHX-1a_16	0.1028	0.0002	0.0015	27.381	1.730	0.108	0.018	−0.881
AHX-1a_17	0.0842	0.0002	0.0008	29.057	1.271	0.106	0.018	−0.622
AHX-1a_18	0.1519	0.0002	0.0008	29.813	0.981	0.082	0.009	−0.711
AHX-1a_19	0.1114	0.0002	0.0007	29.662	0.971	0.082	0.010	−0.545
AHX-1a_20	0.0899	0.0001	0.0006	29.219	1.028	0.086	0.010	−0.656
AHX-1a_21	0.1097	0.0002	0.0006	30.011	0.994	0.071	0.008	−0.713
AHX-1a_22	0.0981	0.0001	0.0009	29.057	1.186	0.101	0.014	−0.737
AHX-1a_23	0.1167	0.0001	0.0010	29.724	0.975	0.099	0.012	−0.616
AHX-1a_24	0.0968	0.0001	0.0010	28.973	1.179	0.107	0.016	−0.770
AHX-1a_25	0.1427	0.0002	0.0020	28.476	1.546	0.119	0.021	−0.905
AHX-1a_26	0.1070	0.0002	0.0014	28.154	1.193	0.107	0.018	−0.804
AHX-1a_27	0.2519	0.0002	0.0009	30.414	0.928	0.068	0.005	−0.423
AHX-1a_28	0.1972	0.0002	0.0312	14.097	0.738	0.500	0.020	−0.897
AHX-1a_29	0.2469	0.0001	0.0636	10.285	0.403	0.594	0.009	−0.722
AHX-1a_30	0.1790	0.0002	0.0673	7.841	0.259	0.660	0.008	−0.136
AHX-1a_31	0.1402	0.0001	0.0011	28.797	0.998	0.084	0.010	−0.742
AHX-1a_32	0.1856	0.0002	0.0008	29.365	0.865	0.066	0.005	−0.156
AHX-1a_33	0.0954	0.0001	0.0012	27.762	1.469	0.104	0.019	−0.754
AHX-1a_34	0.1709	0.0000	0.0007	28.492	0.977	0.071	0.008	−0.647
AHX-1a_35	0.1387	0.0001	0.0007	28.805	0.999	0.081	0.010	−0.599
AHX-1a_36	0.0914	0.0002	0.0011	27.762	1.160	0.110	0.016	−0.741
AHX-1a_37	0.1186	0.0001	0.0009	28.035	1.025	0.083	0.011	−0.794
AHX-1a_38	0.0916	0.0002	0.0006	28.714	0.993	0.077	0.007	−0.152
AHX-1a_39	0.1191	0.0000	0.0011	28.805	1.166	0.088	0.013	−0.766
AHX-1a_40	0.0981	0.0001	0.0009	28.476	1.383	0.098	0.014	−0.676
AHX-1a_41	0.1215	0.0001	0.0008	29.391	1.040	0.083	0.009	−0.734
AHX-1a_42	0.1031	0.0001	0.0009	28.722	1.159	0.091	0.012	−0.687
AHX-1a_43	0.1191	0.0000	0.0009	28.813	1.000	0.083	0.010	−0.446
AHX-1a_44	0.0881	0.0000	0.0008	27.685	1.154	0.098	0.013	−0.691
AHX-1a_45	0.1171	0.0001	0.0010	27.925	1.017	0.094	0.011	−0.590
AHX-1a_46	0.0953	0.0136	0.0007	27.839	1.011	0.089	0.011	−0.603
AHX-1a_47	0.0954	0.0004	0.0006	29.487	1.047	0.092	0.011	−0.494
AHX-1a_48	0.0964	0.0005	0.0007	28.557	1.227	0.089	0.011	−0.752
AHX-1a_49	0.0927	0.0022	0.0006	29.760	1.066	0.085	0.009	−0.337
AHX-1a_50	0.1155	0.0000	0.0009	28.776	0.712	0.090	0.009	−0.588

References

1. Craig, C.H.; Sandwell, D.T. Global distribution of seamounts from Seasat profiles. *J. Geophys. Res.* **1988**, *90*, 10408–10420. [[CrossRef](#)]
2. Wessel, P.; Lyons, S. Distribution of large Pacific seamounts from Geosat/ERS-1: Implications for the history of intraplate volcanism. *J. Geophys. Res.* **1997**, *102*, 22459–22475. [[CrossRef](#)]
3. Wessel, P. Global distribution of seamounts inferred from gridded Geosat/ERS-1 altimetry. *J. Geophys. Res.* **2001**, *106*, 19431–19441. [[CrossRef](#)]
4. Kitchingman, A.; Lai, S.; Morato, T.; Pauly, D. How many seamounts are there and where are they located? In *Seamounts: Ecology, Fisheries & Conservation*; Fock, H.O., Ed.; Blackwell Publishing: Oxford, UK, 2007; pp. 26–40.
5. Staudigel, H.; Koppers, A.A.P. Chapter 22—Seamounts and island building. In *The Encyclopedia of Volcanoes*, 2nd ed.; Sigurdsson, H., Houghton, B.F., McNutt, S.R., Rymer, H., Stix, J., Eds.; Elsevier Inc.: Amsterdam, The Netherlands, 2015; pp. 405–421.
6. Manheim, F.T. Marine Cobalt Resources. *Science* **1986**, *232*, 600–608. [[CrossRef](#)] [[PubMed](#)]
7. Yamazaki, T.; Sharma, R. Distribution characteristics of Co-rich manganese deposits on a seamount in the central Pacific Ocean. *Mar. Georesources Geotechnol.* **1998**, *16*, 283–305. [[CrossRef](#)]
8. Yang, H.; Park, S. A Technical and Economic Evaluation of Cobalt-rich Manganese Crusts. *Ocean Polar Res.* **2009**, *31*, 167–176. [[CrossRef](#)]
9. Okamoto, N.; Usui, A. Regional Distribution of Co-Rich Ferromanganese Crusts and Evolution of the Seamounts in the Northwestern Pacific. *Mar. Georesources Geotechnol.* **2014**, *32*, 187–206. [[CrossRef](#)]
10. Zhang, F.; Zhang, W.; Zhu, K.; Gao, S.; Zhang, H.; Zhang, X.; Zhu, B. Distribution Characteristics of Cobalt-rich Ferromanganese Crust Resources on Submarine Seamounts in the Western Pacific. *Acta Geol. Sin.* **2008**, *82*, 796–803. [[CrossRef](#)]
11. Danovaro, R.; Canals, M.; Gambi, C.; Heussner, S.; Lampadariou, N.; Vanreusel, A. Exploring benthic biodiversity patterns and hotspots on European margin slopes. *Oceanography* **2009**, *22*, 16–25. [[CrossRef](#)]
12. Pitcher, T.J.; Clark, M.R.; Morato, T.; Watson, R. Seamount fisheries: Do they have a future? *Oceanography* **2010**, *23*, 134–144. [[CrossRef](#)]
13. Emerson, D.; Moyer, C.L. Microbiology of seamounts: Common patterns observed in community structure. *Oceanography* **2010**, *23*, 148–163. [[CrossRef](#)]
14. Hein, J.R.; Conrad, T.A.; Staudigel, H. Seamount Mineral Deposits: A Source of Rare Metals for High-Technology Industries. *Oceanography* **2010**, *23*, 184–189. [[CrossRef](#)]
15. Hein, J.R.; Koschinsky, A. 13.11-Deep-ocean ferromanganese crusts and nodules. In *Treatise on Geochemistry*, 2nd ed.; Holland, H.D., Ed.; Elsevier Inc.: Amsterdam, The Netherlands, 2013; Volume 13, pp. 273–291.
16. Liu, Y.; He, G.; Yao, H.; Yang, Y.; Ren, J.; Guo, L.; Mei, H. Global distribution characteristics of seafloor cobalt-rich encrustation resources. *Miner. Depos.* **2013**, *32*, 1275–1284, (In Chinese with English Abstract). [[CrossRef](#)]
17. Wei, Z.; He, G.; Deng, X.; Yao, H.; Liu, Y.; Yang, Y.; Ren, J. The progress in the study and survey of oceanic cobalt-rich crust resources. *Geol. China* **2017**, *44*, 460–472, (In Chinese with English Abstract).
18. Ren, J.B.; He, G.W.; Deng, X.G.; Deng, X.Z.; Yang, Y.; Yao, H.Q.; Yang, S.X. Metallogenesis of Co-rich ferromanganese nodules in the northwestern Pacific: Selective enrichment of metallic elements from seawater. *Ore Geol. Rev.* **2022**, *143*, 104778. [[CrossRef](#)]
19. Staudigel, H.; Clague, D.A. The geological history of deep-sea volcanoes: Biosphere, hydrosphere, and lithosphere interactions. *Oceanography* **2010**, *23*, 58–71. [[CrossRef](#)]
20. Zhao, B.; Lü, W.C.; He, G.W.; Zhang, B.J.; Wei, Z.Q.; Ning, Z.J.; Zhang, X. Sedimentary Processes of the Weijia Guyot and the Implications for Western Pacific Seamounts Evolution. *Earth Sci.* **2022**, *47*, 357–367. [[CrossRef](#)]
21. Cheng, T.; Zhao, J.X.; Feng, Y.X.; Pang, W.Q.; Liu, D.Y. In-situ LA-MC-ICPMS U-Pb dating method for low-uranium carbonate minerals. *Chin. Sci. Bull.* **2020**, *65*, 150–154. (In Chinese) [[CrossRef](#)]
22. Kendrick, M.A.; Zhao, J.; Feng, Y. Early accretion and prolonged carbonation of the Pacific Ocean's oldest crust. *Geology* **2022**, *50*, 1270–1275. [[CrossRef](#)]
23. Koppers, A.A.P.; Staudigel, H.; Pringle, M.S.; Wijbrans, J.R. Short-lived and discontinuous intraplate volcanism in the South Pacific: Hot spots or extensional volcanism? *Geochem. Geophys. Geosystems* **2003**, *4*, 1–49. [[CrossRef](#)]
24. Staudigel, H.; Park, K.H.; Pringle, M.; Pringle, M.; Rubenstone, J.L.; Smith, W.H.F.; Zindler, A. The longevity of the South Pacific Isotope and Thermal Anomaly. *Earth Planet. Sci. Lett.* **1991**, *102*, 24–44. [[CrossRef](#)]
25. Koppers, A.A.P.; Staudigel, H.; Christie, D.M.; Dieu, J.J.; Pringle, M.S. Sr-Nd-Pb Isotope Geochemistry of Leg 144 West Pacific guyots: Implications for the geochemical evolution of the 'SOPITA' mantle anomaly. *Proc. Ocean. Drill. Program Sci. Results* **1995**, *144*, 535–545.
26. Koppers, A.A.P.; Staudigel, H.; Wijbrans, J.R.; Pringle, M.S. The Magellan seamount trail: Implications for Cretaceous hotspot volcanism and absolute Pacific plate motion. *Earth Planet. Sci. Lett.* **1998**, *163*, 53–68. [[CrossRef](#)]
27. Shen, A.; Hu, A.; Cheng, T.; Liang, F.; Pan, W.; Feng, Y.; Zhao, J. Laser ablation in situ U-Pb dating and its application to diagenesis-porosity evolution of carbonate reservoirs. *Pet. Explor. Dev.* **2019**, *46*, 1127–1140. [[CrossRef](#)]
28. Paton, C.; Hellstrom, J.; Paul, B.; Woodhead, J.; Hergt, J. Iolite: Freeware for the visualisation and processing of mass spectrometric data. *J. Anal. At. Spectrom.* **2011**, *26*, 2508–2518. [[CrossRef](#)]

29. Lawson, M.; Shenton, B.J.; Stolper, D.A.; Eiler, J.M.; Rasbury, E.T.; Becker, T.P.; Phillips Lander, C.M.; Buono, A.S.; Becker, S.P.; Pottorf, R. Deciphering the diagenetic history of the El Abra Formation of eastern Mexico using reordered clumped isotope temperatures and U–Pb dating. *Geol. Soc. Am. Bull.* **2018**, *130*, 617–629. [[CrossRef](#)]
30. Ludwig, K.R. *User's Manual for Isoplot 3.75: A Geochronological Toolkit for Microsoft Excel*; Special Publication, No. 5; Berkeley Geochronology Center: Berkeley, CA, USA, 2012; p. 75.
31. Wilson, P.A.; Jenkyns, H.C. The paradox of drowned carbonate platforms and the origin of Cretaceous Pacific guyots. *Nature* **1998**, *392*, 889–894. [[CrossRef](#)]
32. Simon, C.; Stephan, J.; Gwenaël, J.; Camoin, G.; Boudagher-Fadel, M.K.; Bachèlery, P.; Caline, B.; Boichard, R.; Sidonie, R.; Yannick, T.; et al. Impact of tectonic and volcanism on the Neogene evolution of isolated carbonate platforms (SW Indian Ocean). *Sediment. Geol.* **2017**, *355*, 114–131.
33. Takayanagi, H.; Iryu, Y.; Yamada, T.; Oda, M.; Yamamoto, K.; Sato, T.; Chiyonobu, S.; Nishimura, A.; Nakazawa, T.; Shiokawa, S. Carbonate deposits on submerged seamounts in the northwestern Pacific Ocean. *Isl. Arc* **2007**, *16*, 394–419. [[CrossRef](#)]
34. Seton, M.; Müller, R.D.; Zahirovic, S.; Gaina, C.; Torsvik, T.; Shephard, G.; Talsma, A.; Gurnis, M.; Turner, M.; Maus, S.; et al. Global continental and ocean basin reconstructions since 200 Ma. *Earth-Sci. Rev.* **2012**, *113*, 212–270. [[CrossRef](#)]
35. Wei, Z.Q.; Yang, Y.; He, G.W.; Yang, S.X.; Yao, X. Drift history and subsidence process of Weijia Guyot, China contract area of Co-rich crust. *Geol. Bull. China* **2021**, *40*, 260–266. (In Chinese)

Disclaimer/Publisher's Note: The statements, opinions and data contained in all publications are solely those of the individual author(s) and contributor(s) and not of MDPI and/or the editor(s). MDPI and/or the editor(s) disclaim responsibility for any injury to people or property resulting from any ideas, methods, instructions or products referred to in the content.